First-principles investigations of caloric effects in ferroic materials

Peter Entel, Sanjubala Sahoo, Mario Siewert, Markus E. Gruner, Heike C. Herper et al.

Citation: AIP Conf. Proc. **1461**, 11 (2012); doi: 10.1063/1.4736867
View online: http://dx.doi.org/10.1063/1.4736867
View Table of Contents: http://proceedings.aip.org/dbt/dbt.jsp?KEY=APCPCS&Volume=1461&Issue=1
Published by the American Institute of Physics.

First-Principles Investigations of Caloric Effects in Ferroic Materials [1]

Peter Entel*, Sanjubala Sahoo*, Mario Siewert*, Markus E. Gruner*, Heike C. Herper*, Denis Comtesse*, Mehmet Acet*, Vasiliy D. Buchelnikov† and Vladimir V. Sokolovskiy†

*Faculty of Physics and CENIDE, University of Duisburg-Essen, 47048 Duisburg, Germany
†Condensed Matter Physics Department, Chelyabinsk State University, 454001 Chelyabinsk, Russia

Abstract.
We study the magnetic interactions in Ni-Mn-based Heusler alloys which are suitable candidates for refrigeration based on magnetocaloric, barocaloric, and elastocaloric effects, where the adiabatic temperature change of the Heusler material is induced by applying a magnetic field, hydrostatic pressure, or compressive strain. The predominantly ferromagnetic interactions of the Heusler alloys with austenite cubic structure at high temperatures are modified by the appearance of antiferromagnetic interactions in the alloys with Mn-excess because of the much shorter distances between the Mn-excess atoms and those on the original Mn-sublattice. This leads to a larger entropy change across the magnetostructural transformation in $Ni_{50}Mn_{25+x}(Ga, In, Sn, Sb)_{25-x}$ alloys and is also responsible for the appearance of the inverse magnetocaloric effect in the martensitic phase. In Ni-excess Ni-Mn-Ga alloys the influence of antiferromagnetic correlations is weaker and the large entropy change across the magnetostructural transition is mainly caused by the disorder introduced in the Mn sublattice by the excess Ni atoms. We find that the magnetocaloric effect and other functional properties like the magnetic shape-memory effect and the exchange bias effect, are goverened by these complex mixed magnetic features.

Keywords: Magnetocaloric effect, Heusler alloys, Density functional theory calculations, Monte Carlo simulations
PACS: 75.30.Sg, 63.70.+h, 75.30.Kz, 75.30.Et

INTRODUCTION

The magnetic Heusler alloys [1] have attracted particular interest in the past years because of their functional properties like the magnetic shape-memory effect (MSME), exchange bias effect (EBE) and magnetocaloric effect (MCE) [2–5]. The wide range of their multifunctional properties, especially the extraordinary magneto-optical, magneto-electronic and exceptional transport properties in relation to basic chemical and physical properties has recently been highlighted in [6]. In addition, the use of half Heuslers as spintronics materials has been anticipated [6, 7]. The MCE is perhaps one of the most promising functional properties. It allows heating or cooling due to the entropy change upon adiabatic magnetization in an external magnetic field [8–11]. This entropy change can be very large across a magnetostructural transformation which is rather common

[1] Dedicated in memory of Prof. Dr. Surjyo N. Behera, Bhubaneswar, India

Functional Materials
AIP Conf. Proc. 1461, 11-23 (2012); doi: 10.1063/1.4736867

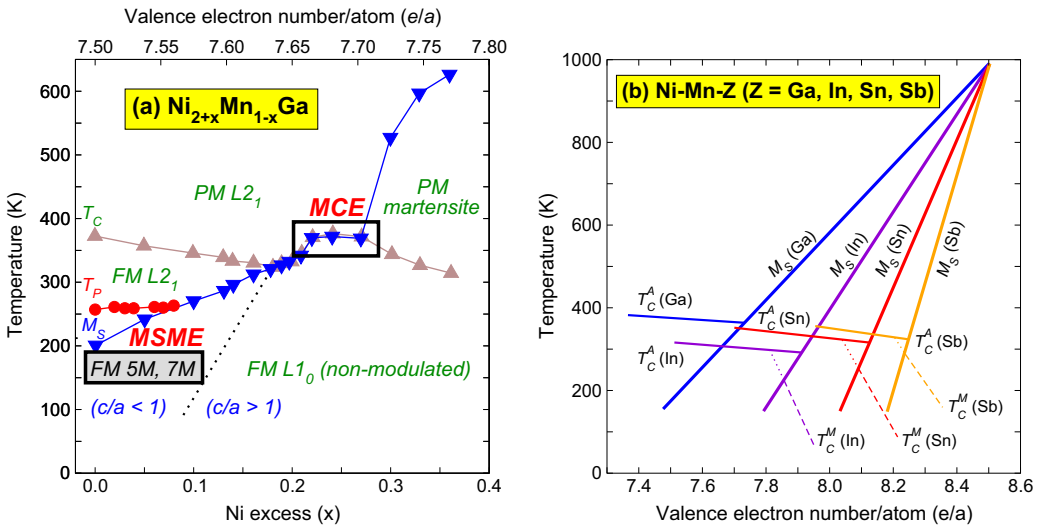

FIGURE 1. (a) Phase diagram of Ni-excess $Ni_{2+x}Mn_{1-x}Ga$ in the temperature versus valence electron concentration plane, $(T, e/a)$. The martensitic transformation and Curie temperatures, T_C and M_S, merge over a substantial range of e/a. PM and FM stand for paramagnetic and ferromagnetic phases, respectively. c/a smaller and larger than one indicate the different regions of tetragonal distortions. T_P denotes the premartensitic transition temperature. Regions of MSME and MCE are highlighted. Phase diagram adapted from [16]. (b) Phase diagram of $Ni_{50}Mn_{25+x}(Ga, In, Sn, Sb)_{25-x}$ in $(T, e/a)$ plane. Note the linear behavior of M_S and decrease of T_C with increasing e/a which can be discussed in terms of increasing number of antiferromagnetically interacting Mn atoms. Further details are given in [3, 4].

among the "pseudobinary" Heusler series $Ni_{50}Mn_{25+x}(Ga, In, Sn, Sb)_{25-x}$ [12–15].

Although the merging of structural transformation and magnetic transition temperatures is a basic ingredient for a large MCE, an understanding of the merging process is still missing. We show in Fig. 1 the range of composition for which the phase tranitions merge in prototypical $Ni_{2+x}Mn_{1-x}Ga$ alloys with Ni-excess concentration [16]. The interesting regions of the MCE and MSME are highlighted. For comparison, we show in Fig. 2 the phase diagram of the pseudobinary alloy series $Ni_{50}Mn_{25+x}(Ga, In, Sn, Sb)_{25-x}$ (see [3, 4] for details regarding the phase diagram of each alloy system as a function of e/a). Note the linear variation of the martensitc (start) transformation temperature M_S with the valence electron concentration e/a.

In this paper we restrict the *ab initio* investigations to the pseudobinary alloy series mentioned before because of the exceptional case of simultaneous presence of conventional and inverse caloric effect in these alloys.

An important feature is connnected with the $L2_1$ Heusler structure of X_2YZ type (X and Y are transition metals and Z is from the groups III-V of the periodic table) which consists of four interpenetrating fcc lattices. With tetragonal distortion the $L2_1$ structure transforms to the $L1_0$ structure for a complete Bain path as shown in Fig. 2(a, b). In case of $Ni_{50}Mn_{25+x}(Ga, In, Sn, Sb)_{25-x}$ alloys any Mn excess atom will occupy the sites of the Z sublattice which reduces the distance between nearest neighbor Mn atoms and is responsible for the appearance of antiferomagnetically aligned spins. The resulting competition of ferromagnetic (FM) and antifferomagnetic (AFM) like interactions is a

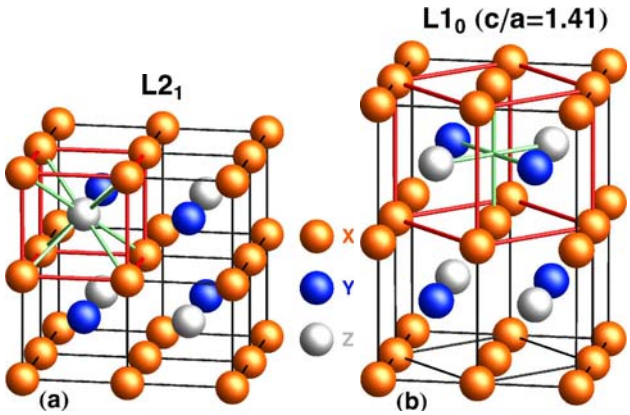

FIGURE 2. (a) $L2_1$ and (b) $L1_0$ structure of the intermetallic Heusler compund X_2YZ (the structure in (b) corresponds to a complete Bain transformation from the bcc-like to the fcc-like structure as highlighted by color). The structure in (a) corresponds to four interpenetrating fcc lattices. The most investigated series is X = Ni, Y = Mn and Z = (Ga, In, Sn, Sb) which exhibits a martensitic transformation from the cubic $L2_1$ structure to tetragonally distorted, orthorhombic or monoclinic modulated structures, respectively. The transformation temperature increases steeply with increasing valence electron number e/a ($e/a = 7.5$ for stoichiometric Ni_2MnGa). For any Mn-exess composition the extra Mn will occupy a lattice site of the previous Z-element since the occupation of the two Ni sublattices does practically not change. This leads to substantially smaller distances between some of the nearest neighbor Mn-pairs which interact now antiferromagnetically.

typical feature of $Ni_{50}Mn_{25+x}(Ga, In, Sn, Sb)_{25-x}$ leading to a layered antiferromagnet for binary NiMn ($x = 25$). The resulting ground state may be non-collinear. The magnetic interactions are strongly involved in the martensitic transformation and affect all physical properties such as MSME, EBE and the MCE. Indeed, the inverse MCE appears because of the breakdown of magnetization below M_S, for example, in Ni-Mn-(In, Sn) alloys.

COMPUTATIONAL DETAILS

Electronic structure calculations are performed using the plane wave pseudopotential DFT method as implemented in the Vienna *ab-initio* simulation package [17–19] together with the generalized gradient approximation (GGA) for the exchange-correlation potential parameterized by Perdew-Burke-Ernzerhof (PBE) [20]. The ion-electron interactions are treated with the projector-augmented wave (PAW) method [19]. The calculations have been done with a sufficiently high energy-cutoff of 460 eV for the plane waves. For the stoichiometric compositions we used 15^3 k-points [21] and the tetrahedron method with Blöchl correction while for off-stoichiometric compositions we used supercells with 16 atoms and 10^3 k-points.

The calculations of the magnetic exchange parameters have been performed by using the Korringa-Kohn-Rostoker (KKR) Green's function method SPR-KKR-CPA code [22].

In the calculations of phase diagrams of $Ni_{50}Mn_{25+x}(Ga, In, Sn, Sb)_{25-x}$ we have

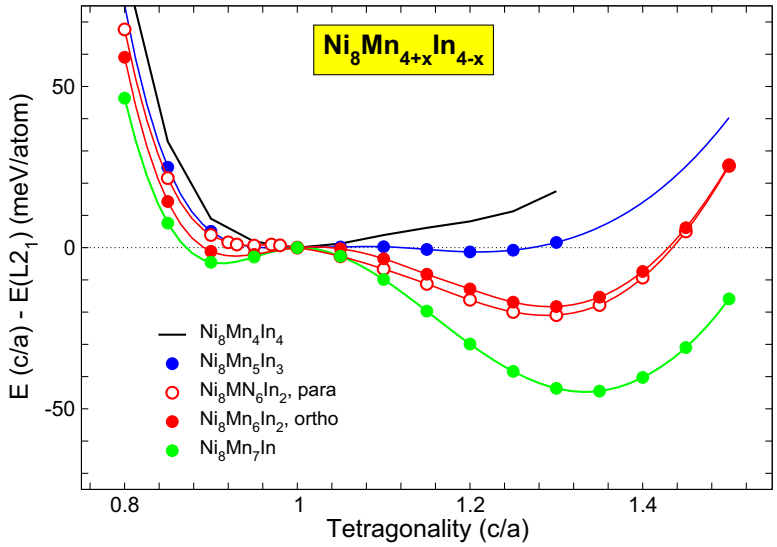

FIGURE 3. Variation of $E(c/a)$ for different compositions of $Ni_8Mn_{4+x}In_{4-x}$ (16-atom supercell). A second energy minimum develops at $c/a < 1$ (for $x > 0$) while the separation in energy between the two minima increases with increasing Mn content (which can be interpreted as tendency for higher M_S). In contrast to Ni_2MnGa stoichiometric Ni_2MnIn is not martensitic. The $E(c/a)$ curves were calculated by keeping the cell volume constant corresponding to the cubic case ($c/a = 1$) because the volume does practically not change when passing from $L2_1$ to $L1_0$. "Para" and "ortho" refer to the case where for the 16-atom supercell the two In atoms in $Ni_8Mn_6In_2$ can be aligned parallel or orthogonal to the c-axes.

followed two routes. In an approximative scheme we have used the 16-atom supercell Ni_8Mn_{4+x}(Ga, In, Sn, Sb)$_{4-x}$ and calculated from the differences of total energies between cubic $L2_1$ and $L1_0$ structures M_S simply by converting energies to temperatures. Although this is a very rough method, it yields remarkably good results for the slopes of M_S as a function of e/a and reproduces the overall behavior of the phase diagrams [23]. In addition, the magnetic transition temperatures T_C have been evaluated with the help of Monte Carlo simulations using the zero-temperature *ab initio* magnetic exchange parameters as input. Here, the trends of the experimental phase diagrams are well reproduced. In a second step, for Ni-Mn-Ga, we have calculated free energies with finite temperature contributions from phonons on an *ab initio* basis. This yields a phase diagram for Ni-Mn-Ga in very good agreement with experiment [23].

Figure 3 shows the energy versus tetragonal distortion curves, $E(c/a)$, for the case of Ni-Mn-In alloys. With increasing Mn content the energy minimum of the cubic phase of Ni_2MnIn moves from $c/a = 1$ to $c/a < 1$, and the resulting energy separation between the two minima at $c/a < 1$ and $c/a > 1$ increases with increasing e/a which can be related to the increase of the martensitic transformation temperature.

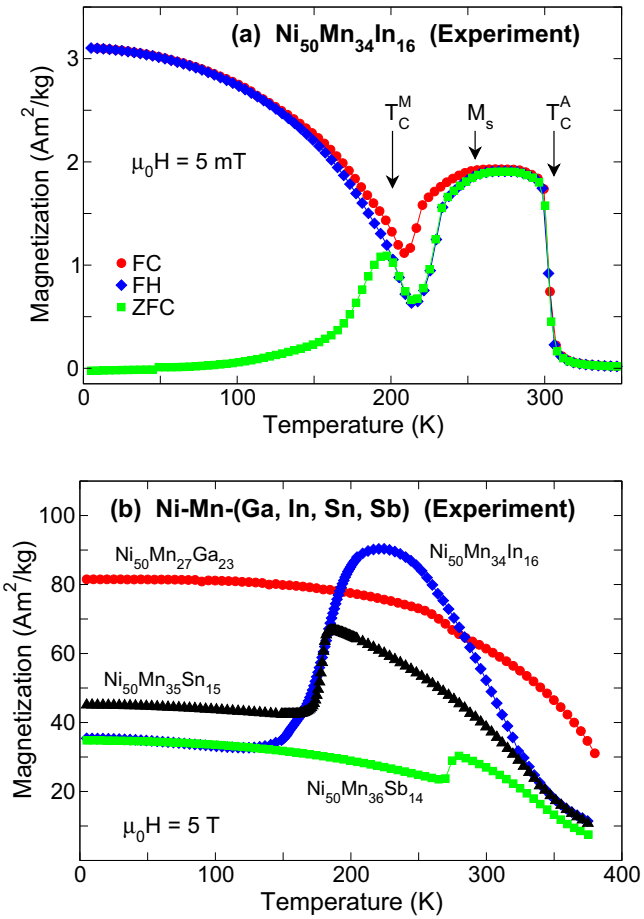

FIGURE 4. (a) Field cooled (FC), field-heated (FH), and zero-field cooled experimental magnetization curves of $Ni_{50}Mn_{34}In_{16}$ at a small magnetic field of $\mu_0 H = 5$ mT. The arrows mark the Curie temperature of the austenitic phase ($T_C^A = 300$ K), the martensitic start temperature ($M_S = 264$ K), and the Curie temperature of the martensitc phase ($T_C^M = 200$ K), respectively. Figure adapted from Ref. [27]. (b) Saturation magnetization curves of $Ni_{50}Mn_{27}Ga_{23}$, $Ni_{50}Mn_{34}In_{16}$, $Ni_{50}Mn_{36}Sn_{15}$, and $Ni_{50}Mn_{36}Sb_{14}$ at $\mu_0 H = 5$ T. For further discussion, see [3, 4, 27].

MAGNETOCALORIC EFFECTS IN NI-MN-(GA, IN, SN. SB) HEUSLER ALLOYS

The Ni-Mn-based alloy series Ni-Mn-(Ga, In, Sn, Sb) is not only of interest concerning applications of relevant magnetic-field-induced (MFI) strains but the investigations have also led to the observation of giant MCE [24–30]. In particular, $Ni_{50}Mn_{34}In_{16}$, $Ni_{45}Co_5Mn_{36.7}In_{13.3}$ and $Ni_{50}Mn_{50-x}Sn_x$ with $x = 13,\ 15$ undergo a martensitic transformation around 250 K and exhibits a field-induced reverse martensitic transformation and an inverse MCE below M_S [26–30].

The drop in the $M(T)$ curves below M_S shown in Fig. 4 is characteristic for all Ni-Mn-Z alloys when measured in low enough external fields and can be associated with

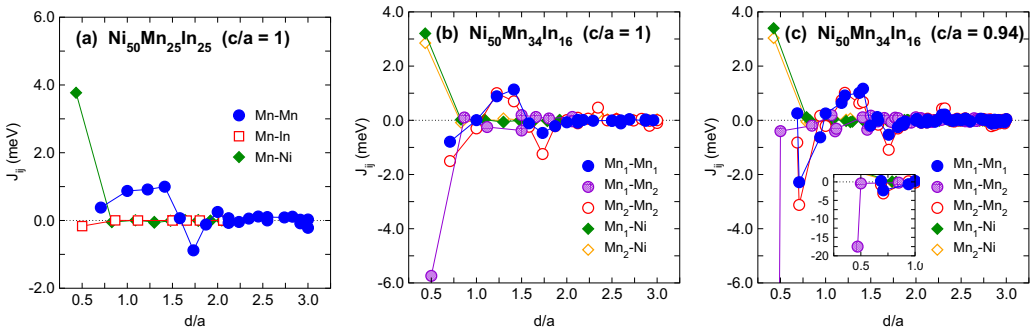

FIGURE 5. The magnetic exchange parameters of $Ni_{50}Mn_{34}In_{16}$ as a function of the distance between the atoms in units of the lattice constant a as obtained from *ab initio* calculations using the SPR-KKR code [22] (see also Ref. [31]). Positive J_{ij} denote ferromagnetic interactions, negative ones are antiferromagnetic interactions. The first of the elements listed in the panel is at the origin, the second one is a distance d/a apart. (a) highlights the results for the stoichiometric compound in the cubic phase while (b) shows the results for the off-stoichiometric composition in the cubic phase and (c) for the off-stoichiometric composition and a tetragonally disorted lattice ($c/a = 0.94$). The increase of the strength of antiferromangetic interactions from (a) to (c) can be clearly noticed.

the appearance of strong AFM correlations. The AFM correlations have two origins. Increasing disorder in the alloys with increasing e/a leads to an increasing occupation of the Z sublattice with Mn. These Mn have nearest neighbor distances to the Mn on the original Mn sublattice which is $a_0/2$ instead of $\sqrt{2}a_0/2$ on the Mn sublattice which switches the magnetic interaction from FM to AFM one. Due to atomic disorder, the competing FM and AFM interactions are present at all temperatures. The second origin is the slight change of nearest neighbor distances due to tetragonal distortions (either $c/a < 1$ or $c/a > 1$). This also favors AFM over FM interactions and is confined to temperatures below M_S. The change of magnetic interactions can be rather drastic as shown in Fig. 5 for the Ni-Mn-In alloys where the change is larger compared to the Ni-Mn-Ga case. The AFM tendencies increase even further for the Ni-Mn-(Sn, Sb) alloys (see also [14, 31]).

The importance of AFM interaction manifests itself in the way that the disordered Ni-Mn-(In, Sn, Sb) alloys show exchange bias behavior at the borderline to an AFM phase. This will not be discussed further here, but we draw attention to Refs. [32–34] where the exchange bias effects associated with magnetostructural transitions have been experimentally investigated and subsequently modelled by Monte Carlo methods applied to Ni-Mn-(In, Sn, Sb) [35]. Usually, the EBE is observed for systems with FM-AFM interfaces. In Ni-Mn-(In, Sn, Sb) it is observed for the composition range below the magnetostructural transition where strong AFM interactions exist. In general, the EBE disappears above the blocking temperature, T_B ($T_B < T_N$ where T_N is the Néel temperature), this issue must still be investigated for the magnetic Heusler alloys.

Here, we discuss basic features of the magnetocaloric effect in Heusler alloys on the basis of *ab initio* in combination with model calculations which nicely reveal that first-principles calculations may be helpful to design more efficient magnetocaloric materials. In Table I we have listed some of the interesting materials which show a giant

magnetocaloric effect ranging from FeRh [36, 37], $Gd_5(Ge_{1-x}Si_x)_4$ [38], RCo_2 [39, 40], $La(Fe_{1-x}Si_x)_{13}$ [41–43], $MnAs_{1-x}Sb_x$ [44], $MnFeP_{1-x}As_x$ [45, 46], $Co(S_{1-x}Se_x)_2$ [47, 48], $Ni_2MN_{1+x}In_{1-x}$ [26], to MnCoGeB [49]. FeRh is interesting not only because of its giant negative temperature (- 13 K) changes but also because of its elastocaloric effect (- 5 K) [37]. The Gd-based system $Gd_5(Ge_{1-x}Si_x)_4$ is very promising although the composition has to be finely tuned [38]. The Laves phase compounds RCo_2 (R = Y, Lu, Sc) undergo a metamagnetic transition from the paramagnetic state to the ferromagnetic one at a high critical magnetic field and show large effects of spin fluctuations. The first order magnetic phase transition temperature is rather low [40]. $La(Fe_{1-x}Si_x)_{13}$ exhibits an intinerant-electron metamagnetic transition at relatively low magnetic fields above the Curie temperature [41–43]. $MnFeP_{0.45}As_{55}$ has a Curie temperature of about 300 K and shows a field-induced first-order transition which allows magnetic refrigeration at room temperature [45, 46]. CoS_2 is a ferromagnet which displays a first order transition with substitution of S by Se [47, 48]. Ni-Mn-(In, Sn) show the inverse magnetocaloric effect below the martensitic transformation in addition to the conventional MCE at the Curie temperature of austenite which make these alloys interesting for multifunctional application although the adiabatic temperature change, which can be achieved today, is still rather small [26]. In MnCoGeB with B at interstitial site a first-order magnetostructural phase transition (from high temperature hexagonal to low temperture orthorhombic structure) and a giant MCE is observed. Furthermore, Heusler alloys containing many elements as in $N_2Mn_{0.75}Cu_{0.25-x}Co_xGa$ [32] may eventually help to tune and optimize the alloys with "mixed magnetism" for refrigeration [54].

This list is by far not complete but indicates the research following different directions and different materials. The magnetic prototype Ni-Mn-Ga Heusler alloys with composition close to stoichiometry like, for example, $Ni_{51.5}Mn_{22.7}Ga_{25.8}$ [55], have been omitted from the list. Although the entropy change can be quite large, as in $Ni_{53.3}Mn_{20.1}Ga_{20.6}$ [56], the recent investigations show that the full phase transition by the magnetic field can occur only for elevated magnitudes of H. Values for ΔT_{ad} are of the order of a few K [14, 15, 57]. For more discussions of the different materials classes we refer to Ref. [50].

A schematic sketch of the MCE in systems undergoing a first-order magnetic phase transition is shown in Fig. 6. The various aspects of thermodynamic cycling can be found in the literature For example, the performance of Gd in a Sterling cycle was already discussed 30 years ago showing that this cycle can operate at nearly the efficiency of the Carnot cycle [51]. The Brayton and Ericsson cycles have recenltly been discussed using a model description of a magnetic material [52]. A comparison of Carnot, Brayton and Ericsson cycles can be found in Ref. [53]. For further references see [50]. A schematical plot of the last three cycles has been added to Fig. 6. The figure clearly shows that the MCE is most effcient for cases when the isofield lines in the entropy versus temperature plane are as steep as possible which allows the cycles to approach the efficiency of the Carnot cycle.

However, the experimental situation is far from achieving optimum cycles and optimum magnetic refrigerants which is to some extent connected to the large transition hysteresis of some of the materials listed in Table 1, also ΔT_{ad} is very often too small. The identification of a figure of merit for magnetic refrigerants is not as clear as for thermoelectrics where $Z = \sigma S^2 T/\kappa$ (σ is the electrical and κ the thermal conductivity and

TABLE 1. A selection of giant magnetocaloric materials with values of isothermal entropy and adiabatic temperature changes in magnetic fields between 2-5 T. For further details see the literature.

Material	ΔS_{max}**(J/kg·K)**	Δ**T(K)**	**Reference**
FeRh		-13	Nikitin *et al.* [36, 37]
$Gd_5(Ge_{1-x}Si_x)_4$	-19.7	15	Pecharsky & Gschneidner [38]
RCo_2	see [40]		Foldeaki *et al.*, Duc *et al.* [39, 40]
$La(Fe_{1-x}Si_x)_{13}$	$\approx$ -20	$\approx$ 8	Hu *et al.*, Fukamichi *et al.* [41–43]
$MnAs_{1-x}Sb_x$	-30	13	Wada *et al.* [44]
$MnFeP_{1-x}As_x$	-14.5/-18		Tegus *et al.* [45, 46]
$Co(S_{1-x}Se_x)_2$	-6		Yamada & Goto, Wada *et al.* [47, 48]
Ni_2Mn_{1+x}(In, Sn)$_{1-x}$	13	$\approx$ -1	Krenke *et al.* [26, 27]
$Ni_{45}Co_5Mn_{36.6}In_{13.6}$	15.2		Kainuma *et al.* [28]
MnCoGeB	-40		Trung *et al.* [49]
$Ni_2Mn_{0.75}Cu_{0.25-x}Co_xGa$	-20		Khan *et al.* [32]

S the thermopower), although one may consider

$$\Delta T_{ad}(T,H) \approx \frac{T\Delta S_{iso}^{mag}(T,H,P,x)}{C(T,H,p,x)} \tag{1}$$

as the corresponding quantity which should be optimized. Here $\Delta S_{iso}^{mag}(T,H,p,x)$ is the dominant (isothermal) magnetic contribution to the entropy change associated with the magnetostructural transition when changing the magnetic field from zero to H, p is the external pressure and x defines the composition of the alloy, while $C(T,H,p,x)$ in the denominator is the total specific heat consisting of the large lattice contribution and the much smaller magnetic contribution. There have been several attempts to optimize $\Delta T_{ad}(T,H)$ yielding expressions like (see Ref. [58] and references therein)

$$\Delta T_{ad}^{max} = \frac{T\Delta S_{iso}^{max}}{C_p} = \frac{T}{C_p}\frac{M_{sat}}{(\partial T_C/\partial H)}, \tag{2}$$

where M_{sat} is the saturation magnetization and the denominator contains the change of Curie temperature with magnetic field. For mixed magnets like the Heusler alloys and especially for the inverse magnetocaloric effect this relation is not really satisfying. It also does not give a remedy for finding new and better magnetic refrigerants. Another popular concept uses the relative cooling power (RCP), which examines the available temperature range of ΔS, to characterize the magnetic refrigerants. But neither the concept of RCP nor plots like $|\Delta S_{ad}^{max}|$ versus $|\Delta S_{iso}^{max}|$ help to find guidelines for improving the magnetic refrigerants.

In the following, we briefly discuss a microscopic model [12–15]. which may help to improve the situation.

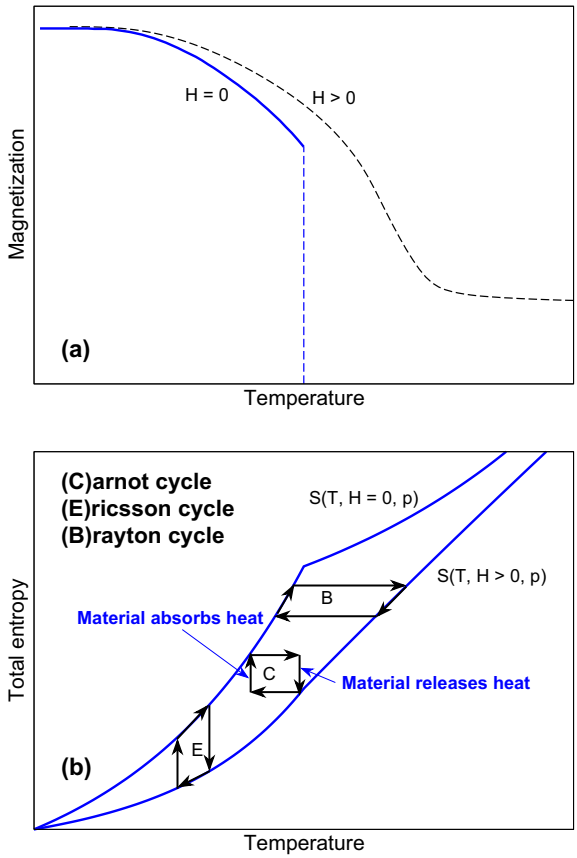

FIGURE 6. (a) Schematic plot of the magnetic order parameter over a first-order magnetostructural phase transition in zero and finite magnetic field. Note that the $M(T)$ curves of the Heusler alloys show characteristic differences, *cf.* Fig. 4. (b) Schematic plot of the total entropy versus temperature along two isofield lines at constant pressure around the first-order mangetostructural phase transition. Three different cycles are shown: Carnot (two isothermal and two adiabatic processes), Ericsson (two isothermal and two isofield processes), and Brayton (two adiabatic and two isofield processes) which may be used in refrigeration devices.

FIRST-PRINCIPLES BASED MODEL DESCRIPTION OF THE MAGNETOCALORIC EFFECT

The isothermal entropy change associated with a magnetic transition in a material may be particularly large when the phase transition goes hand in hand with a structural change of the crystalline lattice leading to a first-order magnetostructural phase transformation. This requires the modelling of magnetostructural coupling which we have successfully applied to Ni-Mn-(Ga, In, Sn, Sb) alloys [12–15]. The corresponding Hamiltonian combines the magnetic degrees of freedom in the framework of a 3-5 Potts model for Ni (spin 1) and Mn (spin 2) with the lattice degrees of freedom using the Blume-Emery-Griffith type of model [59] to describe cubic austenite and tetragonal martensite. It is a generalization of the model which Cástan *et al.* have successfully applied to martensitic

transformations in Ni_2MnGa [60].

$$\begin{aligned}
\mathscr{H} &= \mathscr{H}_m + \mathscr{H}_{lat} + \mathscr{H}_{int}, && (3)\\
\mathscr{H}_m &= -\sum_{\langle ij\rangle} J_m(i,j)\,\delta_{S_i,S_j} - g\mu_B H_{ext}\sum_i \delta_{S_i,S_g}, && (4)\\
\mathscr{H}_{lat} &= -J\sum_{\langle ij\rangle}\sigma_i\sigma_j - K\sum_{\langle ij\rangle}(1-\sigma_i^2)(1-\sigma_j^2) - k_BT\ln(p)\sum_i(1-\sigma_i^2) && (5)\\
&\quad - K_1 g\mu_B H_{ext}\sum_i \delta_{\sigma_i,\sigma_g}\sum_{\langle ij\rangle}\sigma_i\sigma_j, && (6)\\
\mathscr{H}_{int} &= 2U\sum_{\langle ij\rangle}\delta_{S_i,S_j}\left(\tfrac{1}{2}-\sigma_i^2\right)\left(\tfrac{1}{2}-\sigma_j^2\right) - \tfrac{1}{2}U\sum_{\langle ij\rangle}\delta_{S_i,S_j}. && (7)
\end{aligned}$$

Here, $J_m(i,j)$ are the magnetic exchange parameters which are obtained from first-principles calculations and which may develop strong antiferromangetic contributions in the martensitic phase. The Kronecker symbol restricts the spin-spin intraction in the Potts model to the same nearest neighbor q_{MN} and q_{Ni} states of Mn and Ni, respectively. The following Kronecker symbol couples the magnetic field to a specific spin called "ghost spin" (see [14, 15] for details). J and K are structural coupling constants where $\sigma = 0, \pm 1$ includes cubic and tetragonally distorted structures. The cubic state is taken to be p-fold degenerate to account for the high entopy of lattice vibrations of the cubic phase. The logarithmic term can be considered as a temperature dependent crystal field arising from the augmentation of the cubic state. The coupling of the "ghost strain" to the magnetic field allows to favor martensitic variants. Finaly, the sum over σ_i defines the strain order parameter. See [14, 15] for more discussion and computational details. In order to discuss the MCE, we have to evaluate the magnetic part of specific heat and entropy and the lattice contribution to the specific heat where we use the Debye approximation:

$$\begin{aligned}
C_{mag}(T,H) &= \frac{1}{k_bT^2}\left[\left\langle\mathscr{H}^2\right\rangle - \left\langle\mathscr{H}\right\rangle^2\right], && (8)\\
S_{mag}(T,H) &= \int_0^T dT'\frac{C_{mag}(T',H)}{T'}, && (9)\\
C_{lat}(T,\Theta_D) &= 9RN_i\left(4\left(\frac{T}{\Theta_D}\right)^3\int_0^{\theta_d/T}dx\frac{x^3}{e^x-1} - \left(\frac{\Theta_D}{T}\right)\frac{1}{e^{\Theta_D/T-1}}\right), && (10)
\end{aligned}$$

where R is the gas constant, N_i the number of ions per formula unit and θ_D the Debye temperature. The isothermal entropy and adiabatic temperature changes by switching on a magnetic field can be obtained from

$$\begin{aligned}
\Delta S_{mag}(T,H) &= S_{mag}(T,H) - S_{mag}(T,0), && (11)\\
\Delta T_{ad}(T,H) &= -T\frac{\Delta S_{mag}(T,H)}{C(T,H)}. && (12)
\end{aligned}$$

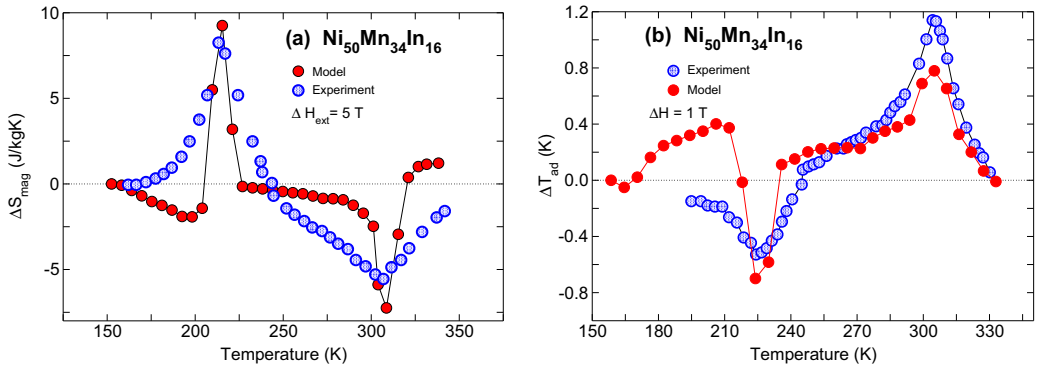

FIGURE 7. Theoretical modelling of (a) ΔS_{mag} and (b) ΔT_{ad} in comparison to experimental data for $Ni_{50}Mn_{34}In_{16}$. The figures show the conventional MCE at the onset of magnetism in the autenitic phase around 300 K as well as the inverse MCE in the martensitic phase below M_S, compare Fig. 4. In the modelling we have used the *ab initio* magnetic exchange paarameters of the cubic and tetragonally distorted phases, compare Fig. 5.

We have applied this model, based on *ab initio* parameters, like the magnetic exchange parameters, where possible, to a series of Heusler alloys. The *ab initio* parameters may be tuned to optimize the MCE for the various alloys. Here, we only show the results for the Ni-Mn-In alloy, which nicely demonstrates that such modelling allows us to describe both the conventional and the inverse magnetocaloric effect, see Fig. 7.

CONCLUSIONS

In this paper we have shown that first-principles calculations of magnetic exchange prameters of the austenitic and martensitic phases when used in an effective spin model (3-5 states Potts model for Ni-Mn-(Ga, In, Sn, Sb) alloys) allow to calculate the thermodynamic relations which govern the magnetocaloric effect. In fact, we have shown that we can reproduce both the conventional as well as the inverse MCE in $Ni_{50}Mn_{34}In_{16}$ by the model calculations in agreement with the experimental data. This also gives a hint of how to improve the MCE from the theoretical side. By substitution and doping we can manipulate the competition of FM and AFM exchange interactions, which decisively influences the magnetocaloric characteristics of each material. This is under present consideration. The importance of magnetic correlations in the Ni-Mn-based Heusler alloys and the possibility of tuning the magnetocaloric properties has also been highlighted in recent experimental work [61, 62].

ACKNOWLEDGMENTS

P. E, would likde to thank the organizers of the IWFM-2011 for the invitation. We acknowledge the computational resources from the Center for Computational Sciences and Simulation (CCSS), of the University of Duisburg-Essen, and the Jülich Supercomputing Centre (JSC) (Blue Gene/L). This work has been performed within the DFG Priority

Programme 1239 “Change of microstructure and shape of solid materials by external magnetic fields”.

REFERENCES

1. P. J. Webster and K. R. A. Ziebeck, in *Magnetic Properties of Metals*, Landolt-Börnstein, New Series, vol. III/32 C, Springer, Berlin (2001), pp. 64-414.
2. A. Planes, L. Mañosa, and A. Saxena (Eds.), *Magnetism and Sructure in Functional Materials*, Springer Series in Materials Science, vol. 79, Springer, Berlin (2005).
3. A. Planes, L. Mañosa, and M. Acet, J. Phys.: Condens. Matter **21**, 233201 (2009).
4. M. Acet, L. Mañosa, and A. Planes, in *Handbook of Magnetic Materials*, vol. 19, K. H. J. Buschow (Ed.), Elsevier, Amsterdam (2011), pp. 231-283.
5. P. Entel, M. E. Gruner, A. Hucht, A. Dannenberg, M. Siewert, H. C. Herper, T. Kakeshita, T. Fukuda, V. V. Sokolovskiy, and V. D. Buchelnikov, in *Disorder and Strain-Induced Complexity in Functional Materials*, T. Kakeshita, T. Fukuda, A. Saxena, and A. Planes (Eds.), Springer Series in Materials Science, vol. 148, Springer, Berlin (2012), pp. 19-47.
6. T. Graf, C. Felser, and S. S. P. Parkin, Progr. Solid State Chem. **39**, 1 (2011).
7. *Half-metallic Alloys - Fundamentals and Applications*, I. Galanakis and P. H. Dederichs (Eds.), Lecture Notes in Physics, vol. 676), Springer, Berlin (2005).
8. A. M. Tishin and Y. I. Spichkin, *The Magnetocaloric Effect and its Applications*, IOP, Bristol (2003).
9. K. A. Gschneidner, Jr., V. K. Pecharsky, and V. O. Tsokol, Rep. Progr. Phys. **68**, 1479 (2005).
10. N. A. de Oliveira and P. J. von Ranke, Phys. Rep. **489**, 89 (2010).
11. V. D. Buchel’nikov and V. V. Sokolovskii, Phys. Metals Metall. **112**, 633 (2011).
12. A. N. Vasil’ev, V. D. Buchelnikov, T. Takagi, V. V. Khovailo, and E. I. Estrin, Phys.Usp. **46**, 559 (2003).
13. P. Entel, V. D. Buchelnikov, V. V. Khovailo, A. T. Zaiak, W. A. Adeagbo, M. E. Gruner, H. C. Herper, and E. F. Wassermann, J. Phys. D: Appl. Phys. **39**, 865 (2006).
14. V. D. Buchelnikov, V. V. Sokolovskiy, H. C. Herper, H. Ebert, M. E. Gruner, S. V. Taskaev, V. V. Khovaylo, A. Hucht, A. Dannenberg, M. Ogura, H. Akai, M. Acet, and P. Entel, Phys. Rev. B **81**, 094411 (2010).
15. V. D. Buchelnikov, V. V. Sokolovskiy, S. V. Taskaev, V. V. Khovaylo, A. A. Aliev, L. N. Khanov, A. B. Batdalov, P. Entel, H. Miki, and T. Takagi, J. Phys. D: Appl. Phys. **44**, 064012 (2011).
16. V. V. Khovaylo, V. D. Buchelnikov, R. Kainuma, V. V. Koledov, M. Ohtsuka, V. G. Shavrov, T. Takagi, S. V. Taskaev, and A. N. Vasiliev, Phys. Rev. B **72**, 224408 (2005).
17. G. Kresse and J. Furthmüller, Comput. Mater. Sci. **6** 15 (1996).
18. G. Kresse and J. Furthmüller, Phys. Rev. B **54** 11169 (1996)
19. G. Kresse and D. Joubert, Phys. Rev. B **59** 1758 (1999)
20. J. P. Perdew, K. Bruke, and M. Ernzerhof, Phys. Rev. Lett. **77**, 3865 (1996).
21. H. J. Monkhorst and J. D. Pack, Phys. Rev. B **13**, 5188 (1976).
22. H. Ebert, in *Electronic structure and Physical Properties of Solids*, Lecture Notes in Physics, Vol. 535, H. Dreyssé, Springer, Berlin (1996), pp. 191-246.
23. M. Siewert, M. E. Gruner, A. Dannenerg, A. Chakrabarti, H. C. Herper, M. Wuttig, S. R. Barman, S. Singh, A. Al-zubi, T. Hickel, J. Neugebauer, M. Gilleessen, R. Dronskowski, and P. Entel, Appl Phys. Lett. **99**, 191904 (2011).
24. J. Marcos, A. Planes, L. Mañosa, F. Casanova, X. Battle, A. Labarta, and B. Martinez, Phys. Rev. B **66**, 224413 (2002).
25. L. Pareti, M. Solzi, F. Albertini, and A. Paoluzi, Eur. Phys. J. B **32**, 303 (2003).
26. T. Krenke, E. Duman, M. Acet, E. F. Wassermann, X. Moya, L. Mañosa, and A. Planes, Nature Mater. **4**, 450 (2005).
27. T. Krenke, M. Acet, E. F. Wassermann, X. Moya, L. Mañosa, and A. Planes, Phys. Rev. B **73**, 174413 (2006).
28. R. Kainuma, Y. Imano, W. Ito, Y. Sutou, H. Morito, S. Okamoto, O. Kitakami, K. Oikawa, A. Fujita, T. Kanomata, and K. Ishida, Nature **439**, 957 (2006).

29. Z. D. Han, D. H. Wang, C. L. Zhang, S. L. Tang, B. X. Gu, and Y. W. Du, Appl. Phys. Lett. **89**, 182507 (2006).
30. V. K. Sharma, M. K. Chattopadhyay, and S. B. Roy, J. Phys. D: Appl. Phys. **40**, 1869 (2007).
31. V. D. Buchelnikov, P. Entel, S. V. Taskaev, V. V. Sokolovskiy, A. Hucht, M. Ogura, H. Akai, M. E. Gruner, and S. K. Nayak, Phys. Rev. B **78**,184427 (2008).
32. M. Khan, I. Dubenko, S. Stadler, and N. Ali, J. Appl. Phys. **102**, 113914 (23007).
33. M. Khan, I. Dubenko, S. Stadler, and N. Ali, J. Phys.: Condens. Matter **20**, 235204 (2008).
34. A. K. Pathak, M. Khan, B. R. Gautam, S. Stadler, I. Dubenko, and N. Ali, J. Magn. Magn. Mater. **321**, 963 (2009).
35. V. Buchelnikov, V. Sokolovskiy, I. Taranenko, S. Taskaev, and P. Entel, J. Phys.: Conf. Series **303**, 012084 (2011).
36. S. A. Nikitin, G. Myalikgulyev, M. P. Annaorazov, A. L. Tyurin, A. M. Tishin, and K. A. Asatryan, Phys. Lett. **148**, 363 (1990).
37. S. A. Nikitin, G. Myalikgulyev, M. P. Annaorazov, A. L. Tyurin, R. W. Myndyev, and S. A. Akopyan, Phys. Lett. **171**, 234 (1992).
38. V. K. Pecharsky, K. A. Gschneidner, Jr., Phys. Rev. Lett. **78**, 4494 (1997).
39. M. Foldeaki, A. Giguere, R. Chahine, and T. K. Bose, Adv. Cryogenic Eng. **43**, 1533 (1998).
40. N. H. Duc, D. T. Kim Anh, and P. E. Brommer, Physica B **319**, 1 (2002).
41. F.-X. Hu, B.-G. Shen, H.-R. Sun, and X.-X. Zhang, Chin. Phys. **9**, 550 (2000).
42. K. Fukamichi and A. Fujita, J. Mater. Sci. Technol. **16**, 167 (2000).
43. K. Fukamichi, A. Fujity, adn S. Fujieda, J. Alloys Comp. **408-412**, 307 (2006).
44. H. Wada and Y. Tanabe, Appl. Phys. Lett. **79**, 3302 (2001).
45. O. Tegus, E. Brück, K. H. J. Buschow, and F. R. de Boer, Nature **415**, 150 (2002).
46. O. Tegus, E. Brück, X. W. Li, L. Zhang, W. Dagula, F. R. de Boer, and K. H. J. Buschow, J. Magn. Magn. Mater. **272-276**, 2389 (2004).
47. H. Yamada and T. Goto, Phys. Rev. B **68**, 184417 (2003).
48. H. Wada, K. Tanaka, and A. Tajiri, J. Magn. Magn. Mater. **290-291**, 706 (2005).
49. N. T. Trung, L. Zhang, L. Caron, K. H. J. Buschow, and E. Brück, Appl. Phys. Lett. **96**, 172504 (2010).
50. E. Brück, in *Handbook of Magnetic Materials*, vol. 17, K. H. J. Buschow (Ed.), Elsevier, Amsterdam (2011), pp. 235-291.
51. W. A. Steyert, J. Appl. Phys. **49**, 1216 (1978).
52. W. N. Huang and C. C. Teng, J. Magn. Magn. Mater. **282**, 311 (2004).
53. C. R. Cross, J. A. Barclay, A. J. Degregoria, S. R. Jaeger, J. W. Johnson, in *Advances in Cryogenic Engineering*, vol. 33, Plenum, New York (1988), p. 767-775.
54. N. H. Dung, Z. Q. Ou, L. Caron, L. Zhang, D. T. C. Thanh, G. A. de Wijs, R. A. de Groot, K. H. J. Buschow, and E. Brück, Ad. Energy Mater. **1**, 1215 (2011).
55. F.-X. Hu, B. Shen, and J. Sun, Appl. Phys. Lett. **76**, 3460 (2000).
56. V. Basso, C. P. Sasso, K. P. Skokov, O. Gutfleisch, and V. V. Khovaylo, Phys. Rev. B **85**, 014430 (2012).
57. V. V. Khovaylo, K. P. Skokov, Yu. S. Koshkid'ko, V. V. Koledov, V. G. Shavroy, V. D. Buchelnikov, V. S. Taskaev, H. Miki, T. Takagi, and A. N. Vasilev, Phys. Rev. B **78**, 060403(R) (2008).
58. K. G. Sandeman, *Magnetocloric materials: the search for new systems*, ArXiv: 1201.3113v1 (15 Jan 2012).
59. M. Blume, V. J. Emery, and R. B. Griffiths, Phys. Rev. A **4**, 1071 (1971).
60. T. Cástan, E. Vives, and P.-A. Lindgård, Phys. Rev. B **60**, 7071 (1999).
61. S. Aksoy, T. Krenke, M. Acet, E. F. Wassermann, X. Moya, L. Mañosa, and A. Planes, Appl. Phys. Lett. **91**, 241916 (2007).
62. S. Aksoy, M. Acet, P. P. Deen, L. Mañosa, and A. Planes, Phys. Rev. B **79**, 212401 (2009).